Eur. Phys. J. C (2024) 84:75
https://doi.org/10.1140/epjc/s10052-024-12417-1

THE EUROPEAN PHYSICAL JOURNAL C

Reply

A study of dipolar signal in distant Quasars with various observables

Rahul Kothari[1,2,a], **Mohit Panwar**[3], **Gurmeet Singh**[3], **Prabhakar Tiwari**[4,5], **Pankaj Jain**[6]

[1] Department of Physics and Astronomy, University of the Western Cape, Cape Town 7535, South Africa
[2] Present address: School of Physical Sciences, Indian Institute of Technology Mandi, Mandi, Himachal Pradesh 175005, India
[3] Department of Physics, Indian Institute of Technology, Kanpur 208016, India
[4] National Astronomical Observatories, Chinese Academy of Science, Beijing 100101, People's Republic of China
[5] Present address: Department of Physics, Guangdong Technion–Israel Institute of Technology, Shantou 515063, Guangdong, People's Republic of China
[6] Department of Space, Science and Astronomy, Indian Institute of Technology, Kanpur 208016, India

Received: 15 August 2023 / Accepted: 8 January 2024 / Published online: 24 January 2024

Abstract We study the signal of anisotropy in AGNs/quasars of CatWISE2020 catalogue using different observables. It has been reported earlier that this data shows a strong signal of dipole anisotropy in the source number counts. We test this claim using two independent data analysis procedures and find our number count dipole consistent with the earlier results. In addition to number counts, we test for the anisotropy signal in two other observables – mean spectral index $\bar{\alpha}$ and mean flux density $\bar{S}$. We find a strong dipole signal both in the mean spectral index and the mean flux density. The dipole in mean flux density points towards the galactic center and becomes very weak after imposing a flux cut to remove sources with flux greater than 1 mJy. This can be attributed to the presence of some ($\sim$ 26,600) bright sources. The signal in the mean spectral index, however, is relatively stable as a function of both flux and galactic cuts. The dipole in this observable points roughly opposite to the galactic center and hence most likely arises due to galactic bias. We consider a simple model of galactic extinction which nicely explains the dipole both in mean spectral index and mean flux density for a wide range of flux and galactic cuts. Hence, the signal in both these parameters does not appear to be of cosmological origin.

1 Introduction

The Standard Model of Cosmology, aka ΛCDM, summarizes our current understanding of the Universe. One of the underlying assumptions of the model is the Cosmological Principle [1–6], according to which the Universe is statistically isotropic and homogeneous at sufficiently large length scales [7,8]. The precise value of this distance is still not clear but is expected to be 100 Mpc or larger [3]. Additionally, the principle is expected to hold in a special frame [9,10] called the Cosmic Rest Frame (CRF henceforth). In this frame, all cosmological observables are expected to be statistically isotropic. Because the solar system is moving with respect to this frame, several cosmological observables, including the large scale structure (LSS) and the cosmic microwave background (CMB), are expected to exhibit dipole anisotropy in this frame due to Doppler shift and aberration effect [11,12]. The dipole in the CMB has been measured very accurately and has been used to predict our velocity with respect to CRF. The LSS dipole has also been observed, but its magnitude doesn't appear to agree with the velocity predicted by the CMB dipole, indicating a $> 5\sigma$ departure [13] from the cosmological principle [14–18]. In this paper, we revisit the dipole in number counts using the CatWISE2020 catalogue[19] data. In addition to this, we use two other observables – (a) mean spectral index $\bar{\alpha}$ and (b) mean flux density $\bar{S}$. Our analysis is based on the extraction of the first three multipoles from the data. The inclusion of quadrupole accounts for the leakage of dipole power into its neighbouring multipoles when multipole fitting is performed on a masked sky. The power beyond the quadrupole is found to be negligible and hence we have neglected any multipoles beyond the quadrupole in our analysis.

The dipole in LSS has been measured using radio surveys [1,14–17,20–23], as well as quasars, observed at infrared frequencies using the CatWISE2020 catalogue [18]. In all

[a] e-mail: quantummechanicskothari@gmail.com (corresponding author)

cases the dipole is found to be in the direction close to the CMB dipole, which lies in the direction ($l = 264.021° \pm 0.011°$, $b = 48.253° \pm 0.005°$) in galactic coordinates [24]. However, the amplitude of the dipole and the extracted local velocity is found to vary significantly and, in most cases, is not consistent with the prediction based on the CMB dipole. A similar discrepancy is seen in the radio polarized flux [25]. Most of the work on radio surveys use the NVSS catalog [26]. A recent paper [27], which employs VLASS [28] and RACS [29] surveys, finds consistency between number counts and CMB dipole. The dipole signal in quasar number counts, observed at infrared frequencies, [18] appears to show a strong, 4.9σ excess, in comparison to the CMB based prediction. In this case, the dipole amplitude is found to be roughly two times higher as compared to the CMB dipole prediction. We add that both radio and infrared galaxy catalogues show reasonable clustering from moderate to small angular scales and their angular power spectrum is a good fit to standard ΛCDM cosmology [30,31]. So it seems that it is only the dipole and a few nearby large-scale multipoles which are higher and hence anomalous as well.

There are also many other observations which appear to show that the Universe is not statistically isotropic even on very large distance scales. For example Park et al. [32] perform isotropy and homogeneity tests on the SDSS Luminous Red Galaxy sample and find that even at $300\,h^{-1}$ Mpc, the isotropy doesn't seem to hold. In the case of CMB, a potential violation of isotropy has been termed *hemispherical power asymmetry* [33] which is basically the presence of different CMB powers in different hemispheres. It still persists in the data at around 3σ statistical significance [34–38]. A detailed review of isotropy violations is given in Ref. [6]. It is somewhat interesting that several of these observations indicate a preferred direction that is closely aligned with the CMB dipole [39]. In this context, Ref. [13] reports an angle $\approx 45°$ between NVSS and CMB dipole directions. These include the dipole in the radio polarization offset angles [40] and the alignment of the CMB quadrupole and octopole [41,42]. The quasar optical polarizations show an alignment over very large distance scales [43,44]. This alignment also has a tendency to maximize in the direction close to the CMB dipole [39].

If the observed deviations from isotropy are indeed confirmed, they would potentially require a major departure from the standard ΛCDM cosmology. There have been many theoretical attempts to explain these observations [45–54]. Here we mention one potential explanation that requires a minimal departure from the ΛCDM model [55,56] and is based on the existence of superhorizon modes [57,58]. The superhorizon modes have wavelengths much larger than the horizon size and hence do not have much effect on most cosmological observations [57,58]. In order to explain the observed violations of isotropy, these modes are assumed to be aligned with one another beyond a certain length scale, i.e., their wave vectors $\hat{\mathbf{k}}$ point in the same direction. Refs. [59,60] implemented this mechanism by assuming the existence of just one such mode and showed that the observed dipole in large scale structures can be explained. The authors perform the calculation using the conformal Newtonian gauge. An alternate calculation, using gauge invariant formalism, finds a null result for dipole [61] if the superhorizon mode is assumed to be adiabatic. However, for more general perturbations, the CMB dipole is found to be nonzero. Hence the ΛCDM relationship between the CMB dipole and structure dipole is not maintained in general. Such a mode also affects the CMB quadrupole and octopole [55,56] and can potentially explain their observed alignment [41]. Remarkably, this simple model also explains the observed tension in the Hubble parameter [62]. It is rather interesting that this model may emerge from a pre-inflationary phase [63,64]. The Universe need not be isotropic and homogeneous before inflation and is expected to acquire this property within the first inflationary efold.[1] Hence, we expect that at sufficiently large distance scales, the cosmic modes need not follow the cosmological principle. This distance scale corresponds to the wavelength of the modes that left the horizon during the aforementioned early stage of inflation. Hence, it is possible that these observed deviations from isotropy may be pointing towards the physics of such an early stage of inflation. Irrespective of this relationship, this model provides a simple and viable explanation for such observations. The model leads to small anisotropy in many cosmological observables, whose amplitude is expected to be of the order of the dipole in large-scale structures or smaller.

In this paper, we explore the dipole signal in three observables using the CatWISE2020 data. We account for the leakage of dipole power into its adjacent multipole–the quadrupole, and extract the dipole in observables by simultaneously fitting the first three multipoles. The contribution beyond quadrupole is relatively small ($\sim$ 10 times) and can be neglected. Hence, our analysis doesn't consider the octopole and higher multipoles. We revisit the signal in number counts using two methods, different from [18] and thus provide independent validation of their findings. The number counts acquire a dipole distribution due to our motion with respect to the CRF [73]. The analysis in [18] shows that the amplitude of this dipole is much higher than expected on purely kinematic grounds. Given the significance of the effect claimed in [18], it is clearly important to determine its source. Assuming that the signal has a physical origin, it is very likely that other observables may also show an anisotropic behaviour. A study of dipole in other observables

[1] Explicit proofs exist in the case of homogeneous comsologies like Bianchi [65,66], Kantowski Sachs [67–70], also some cases of inhomogeneous cosmologies [71,72].

can help in disentangling the physical origin of the effect. We identify two such observables which we study in detail in this paper. These are:

1. The mean spectral index ($\bar{\alpha}$): The variation of flux density $S(\nu)$ (W m^{-2} Hz^{-1}) as a function of frequency (ν) follows a power law $S(\nu) \propto \nu^{-\alpha}$. Although flux density S changes in two different reference frames, α doesn't. We define the mean spectral index $\bar{\alpha}$ as the sum of spectral indices in a given patch of sky divided by the total number of sources in that patch (see Eq. 1). In the standard Big Bang cosmology that includes inflationary paradigm to account for the observed isotropy, $\bar{\alpha}$ would be distributed isotropically in the sky. It is not expected to get any contribution due to kinematic effects. Hence any anisotropy in this parameter would signal a non-standard cosmology. In general, it is common to assume α isotropic, and conventionally, some authors even employ this observable to signal or correct flux systematics. For example, [13] used α to estimate the effect of the flux calibration systematics in TGSS.
2. The mean flux density ($\bar{S}$): It is obtained by dividing the total flux by the number of sources in any region of the sky (see Eq. 2). If we assume that the integral number counts above a given flux density S show a power law distribution, i.e. $\mathrm{d}N/\mathrm{d}\Omega(>S) \propto S^{-x}$, then $\bar{S}$ would be distributed isotropically [74]. Assuming a kinematic origin of dipole, this observable would get a non-zero contribution only if the number count distribution differs from a pure power law. Else, a dipole in this observable can arise only in a non-standard cosmology.

These two observables are also interesting since they are unaffected by the distribution of sources in the sky. The paper is structured in the following manner. In Sect. 2, we give details of the CatWISE2020 catalogue. After this, we explain our first method; based on a χ^2 minimization, for multipole recovery from the masked sky, in Sect. 3. Our second method is based on an extension of `Healpy fit_dipole` method. We apply this method to number counts N and find consistency between the two methods. The details of the second method are discussed in Appendix A where we also estimate the errors in the quantities of interest by simulations. In Sect. 4, we discuss dipole anisotropy results for N, $\bar{\alpha}$ and $\bar{S}$ obtained using χ^2 method. Further, we study dipole anisotropy in $\bar{\alpha}$ and $\bar{S}$, using both galactic and flux cuts. In $\bar{\alpha}$, we find a strong signal of dipole anisotropy and the direction lies close to the galactic plane. In $\bar{S}$, the dipole signal is found to be strong to mild depending upon the imposed flux and galactic cuts. For the cases where the dipole signal is strong, the direction lies close to the galactic plane. We conclude in Sect. 6.

2 The CatWISE catalogue

The CatWISE2020 catalogue [19] is generated from the *Wide-field Infrared Survey Explorer* (WISE) [75] and *NEOWISE* all-sky survey data [76,77] at infrared wavelengths 3.4μm and 4.6μm in the W1 and W2 bands, respectively. The number of sources in CatWISE2020 catalogue is 1,890,715,640. The CatWISE2020 has 90% completeness at 17.7 mag in $W1$ band and 17.5 mag in $W2$ band. In [78], it is shown that a simple mid-infrared color criterion $W1 - W2 \geq 0.8$ identifies both un-obscured and obscured AGNs. In Ref. [79], authors also selected $\approx$ 1.4 million AGNs/Quasars using a two-color selection criterion from the ALLWISE data, that includes data from all phases (4-Band Cryo, 3-Band Cryo, Post-Cryo NEOWISE phase and reactivation NEOWISE – R) of WISE survey. We adopted the same procedure as mentioned in [18] to select the quasars from the CatWISE2020 catalogue and used the same criterion for cuts on the data. The data in [18] has lower flux cut $S > S_{\mathrm{lowercut}} = 0.085$ mJy. We keep the same lower cut in our analysis as well. Spectral index (α) calculation, as well as correction for Galactic reddening, is also based on the same paper. Various cuts to the data are applied in order to select the best candidates that are supposed to be free from any known systematics and bias. We use `HEALpix` visualization and project data with `NSIDE` 64 for our analysis. The final source count (left) and mask (right) maps are shown in Fig. 1.

3 Methodology

We are interested in studying the dipole signal in three observables (a) number counts N, (b) mean spectral index $\bar{\alpha}$ and (c) mean flux density $\bar{S}$. The dipole in number counts has already been studied earlier [13,18]. In order to study the anisotropy in spectral index we consider the mean value of this variable in a small angular region. We use the `Healpy` pixelation scheme for our analysis. For a given pixel p we define the mean spectral index $\bar{\alpha}_{\mathrm{p}}$ as

$$\bar{\alpha}_{\mathrm{p}} = \frac{1}{N_{\mathrm{p}}} \sum_{i=1}^{N_{\mathrm{p}}} \alpha_{i,\mathrm{p}} \tag{1}$$

here N_{p} is the total number of sources and $\alpha_{i,\mathrm{p}}$ denotes the spectral index of ith source in pixel p. The sum is performed over all the sources in the pixel. Similarly we define the mean flux density $\bar{S}_{\mathrm{p}}$ in pixel p as

$$\bar{S}_{\mathrm{p}} = \frac{1}{N_{\mathrm{p}}} \sum_{i=1}^{N_{\mathrm{p}}} S_{i,\mathrm{p}} \tag{2}$$

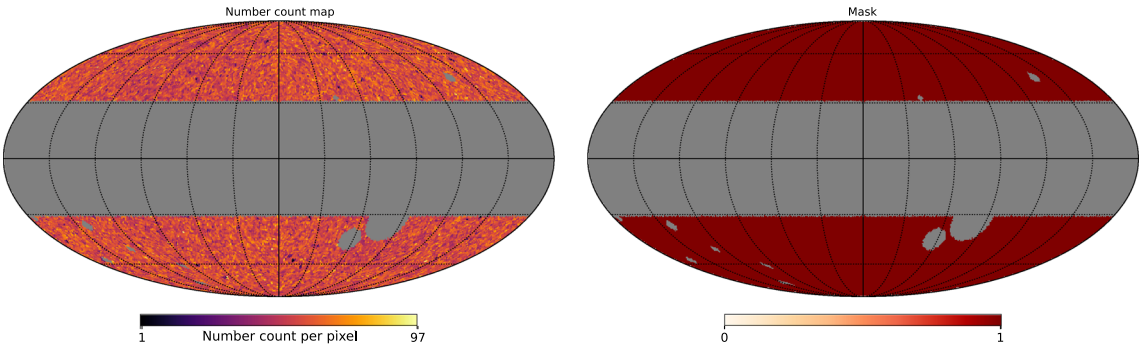

Fig. 1 Left: Number count (i.e., number of sources per pixel) map and Right: the corresponding mask map for CatWISE2020 catalogue after following the masking procedure described in the text

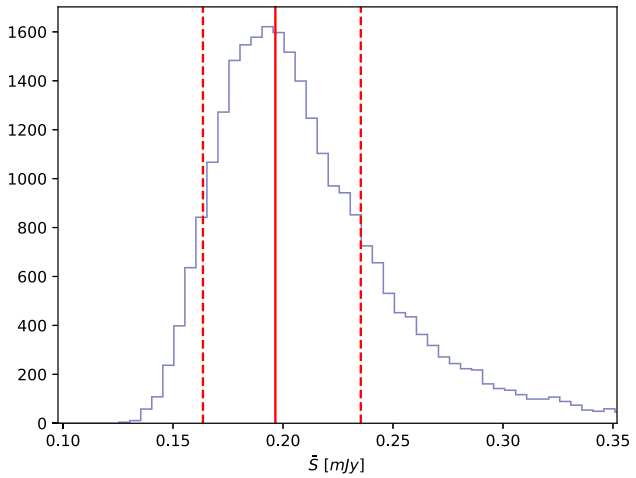

Fig. 2 The distribution of mean flux density $\bar{S}$ from sub-samples. The sub-samples are created by dividing the complete CatWISE catalog into segments, each containing 50 sources. The solid and dashed red lines respectively denote the median, and the one-σ intervals around it

with $S_{i,\mathrm{p}}$ denoting the flux density of ith source in pixel p. We choose only those pixels having ≥ 5 sources. In order to extract the dipole signal we use two different procedures. The χ^2 method is described below while the details of the `Healpy` [80,81] method can be found in Appendix A.

3.1 Multipole expansion

Let $I(\theta, \phi)$ denote a generic quantity of interest (N, $\bar{\alpha}$ or $\bar{S}$) along the direction (θ, ϕ). Assuming that multipoles $\ell \geq 3$ can be neglected, we write

$$\begin{aligned} I(\theta,\phi) \; &= \mathcal{M}_0^{\mathrm{I}} + \mathcal{D}_x^{\mathrm{I}} x + \mathcal{D}_y^{\mathrm{I}} y + \mathcal{D}_z^{\mathrm{I}} z + \mathcal{Q}_{xy}^{\mathrm{I}} xy \\ &\quad + \mathcal{Q}_{xz}^{\mathrm{I}} xz + \mathcal{Q}_{yz}^{\mathrm{I}} yz + \mathcal{Q}_{z^2}^{\mathrm{I}} (2z^2 - x^2 - y^2) \\ &\quad + \mathcal{Q}_{x^2-y^2}^{\mathrm{I}} (x^2 - y^2). \end{aligned} \tag{3}$$

Above equation is basically the spherical harmonic decomposition in the Cartesian basis. Equation (3) contains 9 coefficients – one for monopole ($\mathcal{M}_0$), three for dipole ($\mathcal{D}_x, \mathcal{D}_y, \mathcal{D}_z$), and five for quadrupole ($\mathcal{Q}_{xy}$, $\mathcal{Q}_{xz}$, $\mathcal{Q}_{yz}$, $\mathcal{Q}_{z^2}$, $\mathcal{Q}_{x^2-y^2}$), to be solved for. The superscript I denotes the observable being considered.

The observed dipole for any of the observables **D** is related to the dipole components $\boldsymbol{\mathcal{D}}_i$ present in Eq. (3) as

$$|\mathbf{D}| = \frac{\sqrt{\mathcal{D}_x^2 + \mathcal{D}_y^2 + \mathcal{D}_z^2}}{\mathcal{M}_0}. \tag{4}$$

3.2 The χ^2 statistic

In order to determine the coefficients of Eq. (3), we first divide the whole sky into equal-area pixels using python package `Healpy` and determine the quantity of interest I_{p} for the pixel p. Then we determine the coefficients in Eq. (3) using the χ^2 minimization,

$$\chi^2 = \sum_{\mathrm{p}=1}^{N_{\mathrm{t}}} \left[\frac{I_{\mathrm{p}} - I(\theta,\phi)}{\sigma_{\mathrm{p}}^{\mathrm{I}}} \right]^2, \tag{5}$$

where $\sigma_{\mathrm{p}}^{\mathrm{I}}$ denotes the error in the observable I_{p} in a given pixel p, N_{t} is the number of unmasked pixels, and $I(\theta, \phi)$ is given in Eq. (3).

Although, the source number count follows the Poisson distribution, on account of a large ($\sim 10^6$) number of sources in pixels, it approaches the Gaussian distribution. Thus for the number count map, for a pixel with N_{p} sources, we consider $\sigma_{\mathrm{p}}^{N} = \sqrt{N_{\mathrm{p}}}$. For observables $\bar{\alpha}$ and $\bar{S}$, the distribution is non-trivial and asymmetric. So to determine σ_{p} for these observables, we resort to sub-sampling. For a pixel with n sources, we draw sub-samples with a number count n from the full CatWISE2020 catalogue. Next, we determine the $\bar{\alpha}$ or $\bar{S}$ of these sub-samples. The observed distribution for mean flux density (assuming a pixel has 50 sources) is shown in Fig. 2. In general the distribution will depend upon the value of n, i.e., the number of sources in a given pixel. We notice the skewness in distribution, and draw a 1σ confidence inter-

Table 1 The dipole parameters in the three observables N, $\bar{\alpha}$ and $\bar{S}$ obtained using the quadrupole χ^2 method. The data is tabulated as a function of flux cut $S < S_{\rm cut}$ (in mJy). Angles are shown in degrees. For the source number counts N, it can be seen that the dipole direction and the magnitude remains consistent in the whole flux cut range. In the entire analysis, we have imposed a lower cut on flux, $S > 0.085$ mJy

$S_{\rm cut}$ (mJy)	∞	10.0	0.7	0.3	0.2
# Sources	1,307,511	1,307,023	1,263,875	1,120,488	953,664
$f_{\rm sky}$	0.4724	0.4724	0.4722	0.4721	0.4718
N					
$\lvert\mathbf{D}\rvert \times 10^{-2}$	1.7 ± 0.2	1.7 ± 0.2	1.8 ± 0.2	1.7 ± 0.2	1.7 ± 0.2
l	239 ± 8	239 ± 8	236 ± 8	237 ± 8	230 ± 8
b	30 ± 6	30 ± 6	29 ± 6	28 ± 6	23 ± 6
$\bar{\alpha}$					
$\lvert\mathbf{D}\rvert \times 10^{-3}$	6.6 ± 1.1	7 ± 1	6.7 ± 1.5	6.5 ± 0.9	6.4 ± 0.7
l	171 ± 6	172 ± 5	167 ± 9	168 ± 12	172 ± 11
b	7 ± 6	9 ± 4	8 ± 5	10 ± 6	10 ± 4
$\bar{S}$					
$\lvert\mathbf{D}\rvert \times 10^{-3}$	12 ± 3	8.2 ± 1.7	2.3 ± 0.9	1.9 ± 0.9	0.6 ± 0.5
l	352 ± 60	356 ± 16	306 ± 89	355 ± 39	304 ± 93
b	10 ± 8	11 ± 17	65 ± 59	42 ± 46	32 ± 39

Table 2 The dipole parameters for the three observables N, $\bar{\alpha}$ and $\bar{S}$ obtained using the quadrupole χ^2 method. The data is tabulated as a function of the galactic cut $b_{\rm cut}$. Notice that the table starts with $b_{\rm cut} = 30°$

$b_{\rm cut}$ (deg)	30	35	40	45	50
# Sources	1,307,511	1,117,078	950,186	767,093	619,814
$f_{\rm sky}$	0.4724	0.4030	0.3426	0.2765	0.2235
N					
$\lvert\mathbf{D}\rvert \times 10^{-2}$	1.7 ± 0.2	1.6 ± 0.2	1.3 ± 0.6	1.4 ± 0.5	1.5 ± 0.4
l	239 ± 8	240 ± 9	235 ± 27	227 ± 27	225 ± 21
b	30 ± 6	28 ± 5	34 ± 5	33 ± 13	28 ± 9
$\bar{\alpha}$					
$\lvert\mathbf{D}\rvert \times 10^{-3}$	6.6 ± 1.1	7.4 ± 1.5	6 ± 1	5.4 ± 1.4	3.6 ± 1.8
l	171 ± 6	161 ± 9	172 ± 14	150 ± 14	147 ± 26
b	7 ± 6	5 ± 6	4 ± 5	7 ± 10	14 ± 15
$\bar{S}$					
$\lvert\mathbf{D}\rvert \times 10^{-3}$	12 ± 3	15.1 ± 1.7	10.4 ± 1.8	4.5 ± 1.8	14 ± 15
l	352 ± 60	357 ± 2	23 ± 8	351 ± 149	304 ± 53
b	10 ± 8	7 ± 2	18 ± 5	37 ± 22	21 ± 35

val around the median and determine asymmetric error bars, i.e., $\sigma_{\rm p}^{(\pm)}$. Depending on whether the model's predicted value is larger or smaller than the observed value, we choose $\sigma_{\rm p}^{\rm I}$ equal to $\sigma_{\rm p}^{(+)}$ or $\sigma_{\rm p}^{(-)}$ and perform the χ^2 minimization.

4 Results and discussion

In this section, we give the results of multipole extraction for all three observables using the χ^2 method as a function of flux and galactic cuts. The results have been summarized in Tables 1 and 2. We apply our second method (discussed in 1) to number counts only, as it involves symmetric error bars (see Sect. 3.2).

4.1 Source number counts N

Using χ^2 method, we find the dipole direction $(l, b) = (239° \pm 8°, 30° \pm 6)$. This direction is quite close to the CMB dipole. On the other hand, the magnitude of the dipole is found to be $|\mathbf{D}| = 0.017 \pm 0.002$. This is much larger in comparison to the expected kinematic dipole and is consistent with the value found in [13] that was obtained by a different data analysis procedure. The extracted quadrupole in number counts is shown in Fig. 3 (top row left). As we can see from the figure, it broadly aligns with the ecliptic poles, indicating systematic bias as already noted in [13,18]. In our procedure, we do not need to model this bias since the quadrupole is directly extracted from the data along with the dipole. Though, it is still possible that the bias may not be completely accounted for even after including the quadrupole.

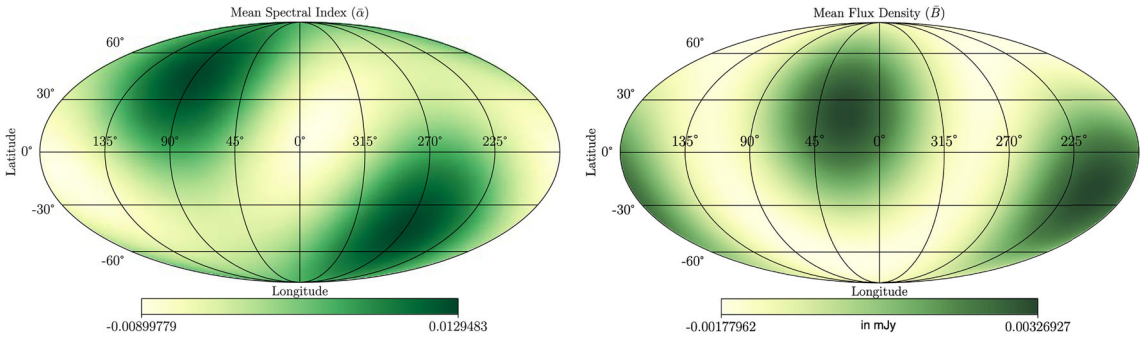

Fig. 3 The extracted quadrupole for number counts N, mean spectral index $\bar{\alpha}$ and mean flux density $\bar{S}$ (anticlockwise from top left) in the Galactic coordinate system. The units for the mean flux density $\bar{B}$ is mJy. It can be seen from the figure, the number counts quadrupole (top row left) broadly aligns with the ecliptic poles, indicating systematic bias. It is worth noting that this bias has also been corrected for in [13,18] by using a different method

We now make a comparison of χ^2 results with those obtained using `Healpy`. The details of the multipole extraction and error estimation can be found in Appendix A. The results are shown in Fig. 4. These are the histograms of various multipole components obtained using 10,000 simulations. The dipole magnitude and directions are found to be $|\mathbf{D}| = 0.016 \pm 0.002$ and $(l, b) = (238° \pm 8°, 30° \pm 5°)$ respectively. Thus we find the results of `Healpy` method are quite close to those obtained using χ^2 method. We've also checked the effect of lower flux cut, $S > S_{\text{lowercut}}$, different from the 0.085mJy. We find no change in the number count dipole, to within error bars.

We have also shown the dependence of extracted monopole $\mathcal{M}_0$ on the order of expansion (Eq. 3) in Table 3, using `Healpy` method. It is important to ascertain that the values of extracted multipole components don't depend upon the order to which we make the expansion in Eq. (3). To this end, we find that $\mathcal{M}_0$ shows no change after $\ell = 2$. We ascribe this to the fact that beyond $\ell = 2$, the angular power spectrum values C_ℓ becomes negligible.

4.1.1 Effect of flux cut

From Table 1, it is clear that the magnitude of dipole as well as direction is very stable and is almost independent of the flux cut imposed. But the error in the quantities increase as we increase the flux cut. The dipole is very significant for all the flux cuts. For number count analysis, we choose only those pixels having > 30 sources.

4.1.2 Effect of galactic cut

In this case too, the dipole magnitude and direction remains almost stable (see Table 2), irrespective of the galactic cut imposed. Further, errors in the quantities increase as the galactic cut is increased. The dipole is very significant for the galactic cuts of 30° and 35°. However, for more stringent galactic cuts, the significance reduces to about 2–3 sigmas.

4.2 Mean spectral index $\bar{\alpha}$

We find a significant signal of dipolar anisotropy in this observable. The dipole amplitude is found to be 0.0066 ± 0.0011 and the direction $l = 171° \pm 6°$ and $b = 7° \pm 6°$. As discussed in Sect. 1, this observable does not get any contribution due to kinematic effects. Thus, the presence of anisotropy in this parameter indicates either a bias or a possible departure from the ΛCDM. We also find a very strong quadrupole in the data, roughly correlated with the ecliptic poles, as shown in Fig. 3 (top row right). This may arise due to observational bias which is also present in number counts. The dipole direction lies close to the galactic plane and points roughly opposite to the galactic center, indicating a possible contamination from our galaxy. In order to study galactic and other sources of contamination in data, we study the effect of (a) flux cut (S_{cut}) and (b) galactic cut (b_{cut}) on this observable.

4.2.1 Effect of flux cut

We study the effect of flux cut $S < S_{\text{cut}}$ as we change S_{cut} from ∞ to 0.1 mJy. The results are given in Table 2. From the table we observe that

1. Both dipole amplitude and the direction remains almost constant till $S_{\text{cut}} = 0.2$ mJy. Further, the dipole direction lies close to the galactic plane and points opposite to the galactic center.
2. At 0.1 mJy cut, the error in both the magnitude and the direction increases considerably. This can be attributed to the drastic change in the number of sources from 953,664 to 302,607 as we go from $S < 0.2$ to $S < 0.1$ mJy. However, within errors, the result remains the same

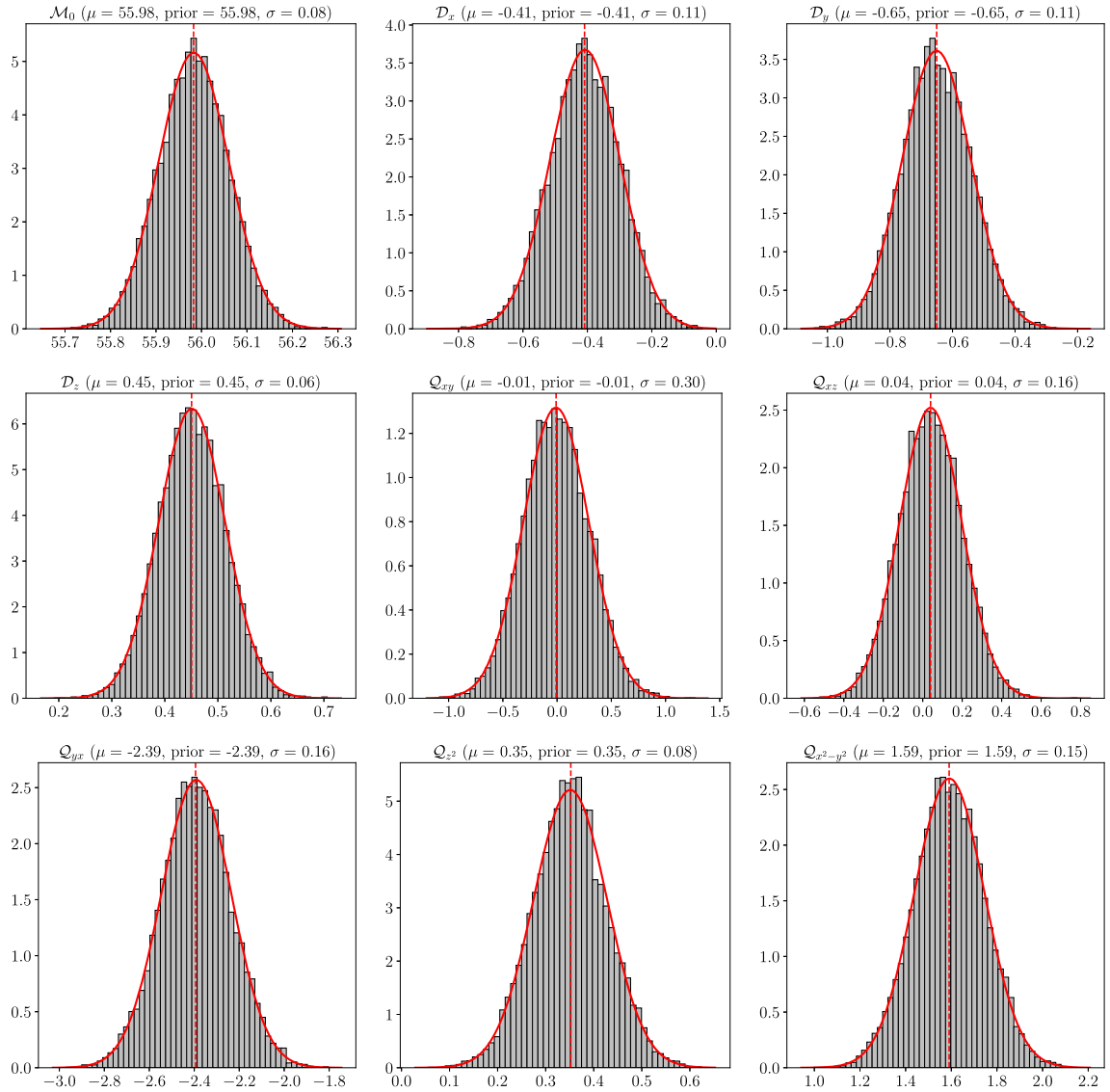

Fig. 4 Distribution histogram of monopole, dipole and quadrupole components (Eq. 3) for source number counts N obtained using `Healpy` method. In the plot, thick vertical dotted lines are priors and thick red curve is the Gaussian fit to the histogram. The corresponding mean (μ) standard deviation (σ) are also shown in the corresponding titles

as with other less stringent flux cuts. The dipole is found to be very significant upto flux cut of 0.2. For the more stringent flux cut of 0.1, the significance becomes smaller than 2 sigmas.

4.2.2 *Effect of galactic cut*

The dipole direction in the mean spectral index is found to be close to the galactic plane, indicating galactic contamination. To explore this further, we study the effect of galactic cut on the observable. This is depicted in Table 2. From the table, we can observe the following

1. For the galactic cut $30° \leq b_{\rm cut} \leq 45°$, we find a very significant dipole signal. The significance is considerably reduced for more stringent galactic cuts $b_{\rm cut} \leq 50°$. The direction for all the cuts in the range $30° \leq b_{\rm cut} \leq 40°$ agrees within errors. It deviates as we impose a more stringent cut $b_{\rm cut} \geq 45°$, but the deviation is not very significant.
2. The effect is not significant for more stringent galactic cuts such as $b_{\rm cut} > 50°$.

Since the effect persists for a wide range of flux cuts, so we cannot attribute it to about 23,600 ($\sim$ 1.7% of all sources) bright sources corresponding to ($S > 1.0$ mJy). The fact

that it points roughly opposite to the galactic center indicates contamination from the galaxy. Hence, it is reasonable to attribute the observed dipole to galactic bias and conclude that the current data is consistent with isotropy in this variable.

4.3 Mean flux density $\bar{S}$

The dipole significance in this case is found to be lower as compared to $\bar{\alpha}$. The dipole amplitude is $(12 \pm 3) \times 10^{-3}$ along $(l, b) = (352^\circ \pm 60^\circ, 10^\circ \pm 8^\circ)$. Here, we find that the direction is towards the galactic center, opposite to what we found in case of $\bar{\alpha}$.

4.3.1 Effect of flux cut

For the flux cuts, the results are again summarised in Table 1. From this table, we observe the following

1. The dipole amplitude and significance suddenly drops after $S_{\text{cut}} = 10$ mJy. This indicates that the dipole signal can be attributed to relatively bright sources in data.
2. For the cases, when the dipole is significant (first two columns), the dipole lies in the galactic plane pointing towards the galactic center
3. In all other cases, the dipole points away from the plane and its significance also reduces

4.3.2 Effect of galactic cut

These results are given in Table 2. From the table, we find that

1. For galactic cuts $b_{\text{cut}} \leq 40$, the dipole is significant. After this, the significance reduces considerably
2. For all galactic cuts, the dipole points approximately towards galactic center and lies close to the galactic plane. The largest deviation from the galactic plane is seen from the cut $b_{\text{cut}} = 45^\circ$

The results clearly suggest that dominant contribution to the dipole arises from relatively bright sources (see discussion just before Sect. 4.3). Furthermore it may get contribution due to galactic contamination.

5 Effect of galactic extinction

The fact that both the mean spectral index $\bar{\alpha}$ and mean flux density $\bar{S}$ dipoles are correlated with the galactic center suggests that the effect may be related to galactic extinction. Here we investigate this possibility through a simple model.

We assume a direction dependent extinction such that

$$I(\nu, \hat{n}) = I(\nu, \theta) = I_0(\nu) e^{-\tau_\nu(\hat{n})} \tag{6}$$

where the optical thickness $\tau_\nu(\hat{n}) = B(\hat{n})\nu$ is assumed to have a dipole angular dependence, i.e., $B(\hat{n}) \propto \hat{n} \cdot \hat{z}$ with z axis taken along the galactic center which is also the direction of mean flux density $\bar{S}$ dipole. The ν dependence is on account of the Mie Scattering Theory (for details see Chapter 12 of [82]). Assuming $\tau_\nu(\hat{n}) \ll 1$, Eq. (6) becomes

$$I(\nu, \hat{n}) \approx I_0(\nu)(1 - \tau_\nu(\hat{n})) = I_0(\nu)\left(1 - B(\hat{n})\nu\right). \tag{7}$$

We have observations at two frequency bands, W1 and W2. For simplicity, we assume that the intensity in each band can be approximated by its central frequency. These frequencies are $\nu_1 = 8.948 \times 10^{13}$ and $\nu_2 = 6.518 \times 10^{13}$ Hz respectively for W1 and W2 bands. We next assume a power law dependence for both $I(\nu, \hat{n})$ and $I_0(\nu)$,

$$I(\nu, \hat{n}) = C(\hat{n})\nu^{-\alpha'} \tag{8}$$

$$I_0(\nu) = A\nu^{-\alpha} \tag{9}$$

where C is direction dependent and A is a constant. Furthermore, since the angle dependent extinction correction is small, we take $\alpha' = \alpha + \delta(\hat{n})$. Applying relations (8) and (9) at frequencies ν_1 and ν_2 and using the fact that $B(\hat{n})(\nu_1 - \nu_2) \ll 1$, we obtain

$$\delta(\hat{n}) = B(\hat{n}) \frac{\nu_1 - \nu_2}{\ln(\nu_1/\nu_2)} \tag{10}$$

This gives us the dipole in the spectral index $\bar{\alpha}$ arising due to extinction. The corresponding dipole in mean flux density $\bar{S}$ is obtained by considering the intensity at W1 band. Using Eq. (7), we obtain

$$\frac{\Delta I(\nu_1, \hat{n})}{I_0(\nu_1)} = \frac{I(\nu_1, \hat{n}) - `I_0(\nu_1)}{I_0(\nu_1)} = -B(\hat{n})\nu_1 \tag{11}$$

Inserting the values of frequencies ν_1 and ν_2 in (10) and (11), we obtain

$$\delta = 7.67 \times 10^{13} B(\hat{n}) \tag{12}$$

$$\frac{\Delta I(\nu_1, \hat{n})}{I_0(\nu_1)} = -8.95 \times 10^{13} B(\hat{n}) \tag{13}$$

From Eqs. (12) and (13), we see that the two dipoles in $\bar{\alpha}$ and $\bar{S}$ are roughly equal in magnitude but opposite in directions. This compares well, within errors, with the observed dipole in these two variables for most of the imposed cuts (see Tables 1 and 2). We can fit the two dipoles and obtain the best fit parameter $\mathcal{B}$ defined by $B = \mathcal{B}\cos\theta$ where θ is the angle measured with respect to z-axis taken to point opposite to the galactic center. For the galactic cut 30°, for example, we obtain the best fit parameter $\mathcal{B} = (0.94 \pm 0.05) \times 10^{-16}\,\text{Hz}^{-1}$

which leads to $\chi^2_{\rm min} = 1.7$ and hence provides a good fit to the data. Here we have assumed that the two axes are aligned with the galactic center with one towards and the other in the opposite direction. The model nicely describes the data with relatively small change in parameters upto galactic cut of 40°. For the more stringent galactic cut 45°, we again find a good fit with $\mathcal{B} = (0.62 \pm 0.14) \times 10^{-16}$ Hz^{-1} with $\chi^2_{\rm min} = 0.55$. The change in parameters can be ascribed to the fact that the sky dependence is likely to be more complicated than a simple dipole. This model also describes the data well up to flux cut $S < 10$ mJy. For more stringent flux cuts, the fit is not good since the model predicts much stronger dipole in $\bar{S}$ in comparison to what is seen in the data. This needs further investigation with more detailed extinction models, which we do not pursue in the current paper.

6 Conclusion and outlook

In this paper, we have studied the dipole in three observables – source number counts, mean spectral index, and mean flux density. We have used two different data analysis methods (χ^2 and `Healpy`) which directly extract the first three multipoles ($\ell = 0, 1, 2$) and the corresponding errors from the data. The higher multipoles are neglected since they are found to be small. The `Healpy` method is applied only for number counts as it involves symmetric error bars. We find results obtained using both methods almost the same. Further, these values are found to be consistent with [13,18]. This provides an independent check on their results. We point out that in our case, we do not model the bias in data associated with the ecliptic pole. This bias leads to a strong quadrupole and is directly extracted from data (https://www.overleaf.com/project/6248739230eccf8d1fbb74dc).

Although the observable N has symmetric error bars, this is no longer true for $\bar{\alpha}$ and $\bar{S}$. Thus we have used only χ^2 method for these observables. Generalization of the `Healpy` method to the non-symmetric error bars can be pursued in future. We find a very strong signal of dipole anisotropy in the mean spectral index $\bar{\alpha}$. The direction in this case lies close to the galactic plane and points roughly opposite to the galactic center. Hence to evaluate the effect of galactic contamination, we study the dipolar anisotropy as a function of the galactic cut. We find that the signal remains very significant for galactic cut $b_{\rm cut} > 45°$ but starts to loose significance for more stringent cuts. We also study the effect of flux cuts $S < S_{\rm cut}$. We find that both the amplitude and direction of the dipole don't show much change as the flux cut is made more stringent. However, as expected, the errors in the dipole parameters become very large for the very stringent flux cut of $S_{\rm cut} = 0.1$ mJy. Since the dipole in this variable points roughly opposite to the galactic center, we conclude that it may be attributed to contamination from our galaxy. We find that it can be nicely explained by a simple model of anisotropic galactic extinction. The model simultaneously explains both the dipole in $\bar{\alpha}$ and $\bar{B}$ for a wide range of cuts. Furthermore, $\bar{\alpha}$ also shows a strong quadrupole roughly correlated with the ecliptic poles, which may indicate the presence of observational bias in data similar to that present in number counts.

The mean flux density $\bar{S}$ also shows a significant dipole with direction pointing towards the galactic center. The dipole becomes considerably reduced and also doesn't remain significant if we impose the flux cut $S_{\rm cut} < 1$ mJy. Additionally, the significance of the dipole reduces beyond the galactic cut $b_{\rm cut} \leq 40°$. For a wide range of flux and galactic cuts, the observed dipole can be nicely explained by a simple empirical model of anisotropic galactic extinction. This model is consistent with the fact that the dipole in $\bar{S}$ points towards the galactic center while that in $\bar{\alpha}$ points in the opposite direction. Hence the dipole in these variables does not appear to be of cosmological origin. Thus we conclude that both the mean spectral index and the mean flux density are consistent with isotropy. The codes (`multipoleFit` and `ChiSquareMinimize`) for generating tables and figures in this paper can be found here .

Acknowledgements We acknowledge the use of `python` packages `scipy` [83], `matplotlib` [84] and `numpy` [85] for our analysis. We are extremely grateful to Nathan Secrest for giving valuable comments on our draft. Rahul Kothari is supported by the South African Radio Astronomy Observatory and the National Research Foundation (Grant No. 75415). PT acknowledges the support of the RFIS grant (No. 12150410322) by the National Natural Science Foundation of China (NSFC). We are also thankful to the anonymous referee whose report helped us improving the quality of the paper.

Data Availability Statement This manuscript has no associated data or the data will not be deposited. [Authors' comment: This manuscript has no associated data].

Funded by SCOAP^3.

Table 3 Comparison of the monopole values $\mathcal{M}_0$ in number counts by considering the expansion for various ℓ values. The monopole value shows no change after $\ell = 2$

	$\ell \leq 0$	$\ell \leq 1$	$\ell \leq 2$	$\ell \leq 3$
$\mathcal{M}_0$	56.29	56.30	55.98	55.98

Appendix A: An alternative method for extracting masked sky multipole coefficients

In this section, we give details of an alternate procedure to extract the multipole coefficients for a given observable. Here, we have applied the method only for number counts map N. First, we talk about extracting the coefficients and then a method for estimating the corresponding errors. In order to better understand the *modus operandi*, we have considered a few special cases. We have also given an example of our procedure in Fig. 4 that shows the distribution of various parameters which is found to be Gaussian to a very good extend. Additionally, we have given corresponding mean values (μ) and standard deviation (σ) for number counts N.

A.1 Coefficients' extraction

The method is based on solving a system of linear equations. In a multipole expansion, considered till ℓ, we'd need $(\ell+1)^2$ equations for obtaining all the coefficients in Eq. (3). Thus in our case, we need to solve a system of 9 linear equations. Although, in our analysis, we have terminated the expansion at $\ell = 2$, yet we must emphasize that the procedure can be generalized to any order. As the first step, we write the discretized version of Eq. (3) (here $r_{\rm p}^2 = x_{\rm p}^2 + y_{\rm p}^2 + z_{\rm p}^2$)

$$\begin{aligned} I_{\rm p} = {} & \mathcal{M}_0^{\rm I} + \mathcal{D}_x^{\rm I}\, x_{\rm p} + \mathcal{D}_y^{\rm I}\, y_{\rm p} + \mathcal{D}_z^{\rm I}\, z_{\rm p} + \mathcal{Q}_{xy}^{\rm I}\, x_{\rm p} y_{\rm p} \\ & + \mathcal{Q}_{xz}^{\rm I}\, x_{\rm p} z_{\rm p} + \mathcal{Q}_{yz}^{\rm I}\, y_{\rm p} z_{\rm p} \\ & + \mathcal{Q}_{z^2}^{\rm I}\, (3z_{\rm p}^2 - r_{\rm p}^2) + \mathcal{Q}_{x^2-y^2}^{\rm I}\, (x_{\rm p}^2 - y_{\rm p}^2) \end{aligned} \tag{A.1}$$

In this equation, $I_{\rm p}$ and $(x_{\rm p}, y_{\rm p}, z_{\rm p})$ respectively denote the observable value and cartesian coordinates of the given pixel in the `Healpy` pixelation scheme. For obtaining these coefficients, we now set up a system of linear equations. To get our first equation, we sum over all the unmasked pixels $N_{\rm t}$ on both sides to get

$$\begin{aligned} \sum_{\rm p=1}^{N_{\rm t}} I_{\rm p} = {} & \mathcal{M}_0^{\rm I} \sum_{\rm p=1}^{N_{\rm t}} 1 + \mathcal{D}_x^{\rm I} \sum_{\rm p=1}^{N_{\rm t}} x_{\rm p} + \mathcal{D}_y^{\rm I} \sum_{\rm p=1}^{N_{\rm t}} y_{\rm p} + \mathcal{D}_z^{\rm I} \sum_{\rm p=1}^{N_{\rm t}} z_{\rm p} \\ & + \mathcal{Q}_{xy}^{\rm I} \sum_{\rm p=1}^{N_{\rm t}} x_{\rm p} y_{\rm p} + \mathcal{Q}_{xz}^{\rm I} \sum_{\rm p=1}^{N_{\rm t}} x_{\rm p} z_{\rm p} \\ & + \mathcal{Q}_{yz}^{\rm I} \sum_{\rm p=1}^{N_{\rm t}} y_{\rm p} z_{\rm p} + \mathcal{Q}_{z^2}^{\rm I} \sum_{\rm p=1}^{N_{\rm t}} (3z_{\rm p}^2 - r_{\rm p}^2) \\ & + \mathcal{Q}_{x^2-y^2}^{\rm I} \sum_{\rm p=1}^{N_{\rm t}} (x_{\rm p}^2 - y_{\rm p}^2) \end{aligned} \tag{A.2}$$

To get the next equation, we multiply (A.1) by $x_{\rm p}$ and then perform the sum. We repeat this process, by multiplying next with $y_{\rm p}$ and so on, i.e., all the direction dependent factors, multiplying multipole coefficients in Eq. (A.1). Finally, we get a system of 9 linear equations which can be written as

$$\mathbb{M}\,\mathbb{P} = \mathbb{N} \tag{A.3}$$

here the parameter vector $\mathbb{P}$ is

$$\mathbb{P} = \left[\mathcal{M}_0^{\rm I}\ \mathcal{D}_x^{\rm I}\ \mathcal{D}_y^{\rm I}\ \mathcal{D}_z^{\rm I}\ \mathcal{Q}_{xy}^{\rm I}\ \mathcal{Q}_{xz}^{\rm I}\ \mathcal{Q}_{yz}^{\rm I}\ \mathcal{Q}_{z^2}^{\rm I}\ \mathcal{Q}_{x^2-y^2}^{\rm I}\right]^T \tag{A.4}$$

and T in the superscript denotes the transpose. The vector $\mathbb{N}$ on the RHS is given by

$$\mathbb{N} = \left[\sum_{\rm p}^{N_{\rm t}} (I_{\rm p}\ I_{\rm p}x_{\rm p}\ I_{\rm p}y_{\rm p}\ I_{\rm p}z_{\rm p}\ I_{\rm p}x_{\rm p}y_{\rm p}\ I_{\rm p}x_{\rm p}x_{\rm p}\ I_{\rm p}y_{\rm p}z_{\rm p}\ I_{\rm p}Z_{\rm p}\ I_{\rm p}M_{\rm p})\right]^T \tag{A.5}$$

where for brevity sake we have defined $Z_{\rm p} = 3z_{\rm p}^2 - 1$, $M_{\rm p} = x_{\rm p}^2 - y_{\rm p}^2$ and the sum outside the parenthesis is meant to be performed on all the terms inside the parenthesis over pixel p. Finally, the symmetric matrix $\mathbb{M}$ is given by the following expression

$$\mathbb{M} = \sum_{\rm p}^{N_{\rm t}} \begin{bmatrix} 1 & x_{\rm p} & y_{\rm p} & z_{\rm p} & x_{\rm p}y_{\rm p} & x_{\rm p}z_{\rm p} & y_{\rm p}z_{\rm p} & Z_{\rm p} & M_{\rm p} \\ x_{\rm p} & x_{\rm p}^2 & x_{\rm p}y_{\rm p} & x_{\rm p}z_{\rm p} & x_{\rm p}^2y_{\rm p} & x_{\rm p}^2z_{\rm p} & x_{\rm p}y_{\rm p}z_{\rm p} & x_{\rm p}Z_{\rm p} & x_{\rm p}M_{\rm p} \\ y_{\rm p} & x_{\rm p}y_{\rm p} & y_{\rm p}^2 & y_{\rm p}z_{\rm p} & x_{\rm p}y_{\rm p}^2 & x_{\rm p}y_{\rm p}z_{\rm p} & y_{\rm p}^2z_{\rm p} & y_{\rm p}Z_{\rm p} & M_{\rm p} \\ z_{\rm p} & x_{\rm p}z_{\rm p} & y_{\rm p}z_{\rm p} & z_{\rm p}^2 & x_{\rm p}y_{\rm p}z_{\rm p} & x_{\rm p}z_{\rm p} & y_{\rm p}z_{\rm p}^2 & z_{\rm p}Z_{\rm p} & z_{\rm p}M_{\rm p} \\ x_{\rm p}y_{\rm p} & x_{\rm p}^2y_{\rm p} & x_{\rm p}y_{\rm p}^2 & x_{\rm p}y_{\rm p}z_{\rm p} & (x_{\rm p}y_{\rm p})^2 & x_{\rm p}^2y_{\rm p}z_{\rm p} & x_{\rm p}y_{\rm p}^2z_{\rm p} & x_{\rm p}y_{\rm p}Z_{\rm p} & x_{\rm p}y_{\rm p}M_{\rm p} \\ x_{\rm p}z_{\rm p} & x_{\rm p}^2z_{\rm p} & x_{\rm p}y_{\rm p}z_{\rm p} & x_{\rm p}z_{\rm p}^2 & x_{\rm p}^2y_{\rm p}z_{\rm p} & (x_{\rm p}z_{\rm p})^2 & x_{\rm p}y_{\rm p}z_{\rm p}^2 & x_{\rm p}z_{\rm p}Z_{\rm p} & x_{\rm p}z_{\rm p}M_{\rm p} \\ y_{\rm p}z_{\rm p} & x_{\rm p}y_{\rm p}z_{\rm p} & y_{\rm p}^2z_{\rm p} & y_{\rm p}z_{\rm p}^2 & x_{\rm p}y_{\rm p}^2z_{\rm p} & x_{\rm p}y_{\rm p}z_{\rm p}^2 & (y_{\rm p}z_{\rm p})^2 & y_{\rm p}z_{\rm p}Z_{\rm p} & y_{\rm p}z_{\rm p}M_{\rm p} \\ Z_{\rm p} & x_{\rm p}Z_{\rm p} & y_{\rm p}Z_{\rm p} & z_{\rm p}Z_{\rm p} & x_{\rm p}y_{\rm p}Z_{\rm p} & x_{\rm p}z_{\rm p} & y_{\rm p}z_{\rm p}Z_{\rm p} & Z_{\rm p}^2 & M_{\rm p}Z_{\rm p} \\ M_{\rm p} & x_{\rm p}M_{\rm p} & y_{\rm p}M_{\rm p} & z_{\rm p}M_{\rm p} & x_{\rm p}y_{\rm p}M_{\rm p} & x_{\rm p}z_{\rm p}M_{\rm p} & y_{\rm p}z_{\rm p}M_{\rm p} & M_{\rm p}Z_{\rm p} & M_{\rm p}^2 \end{bmatrix} \tag{A.6}$$

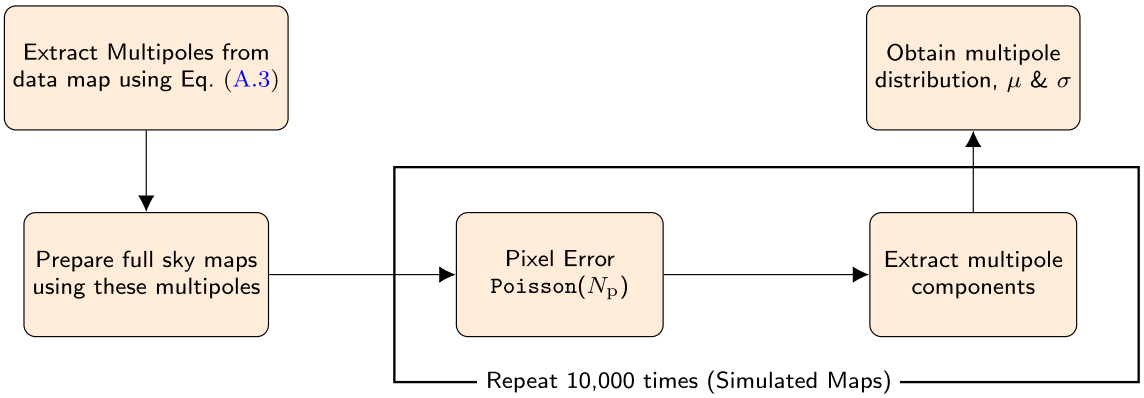

Fig. 5 Algorithm for generating mock maps and multipole extraction for number counts N. For details, the reader is referred to Appendix A.3

A.2 Special cases

In order to gain some insights about the *modus operandi*, it would be useful to consider a few special cases. First we analyze what happens when no pixel is masked. In that case it can be shown that the matrix in Eq. (A.6) becomes diagonal. This is a consequence of the fact that when no pixel is masked

$$\sum_{\text{allpixels}} x_{\rm p}^a y_{\rm p}^b z_{\rm p}^c = 0 \tag{A.7}$$

when either a, b or c are odd. Notice that Eq. (A.7) is a discrete version of the result

$$\iint_{S^2} x^a y^b z^c \, \mathrm{d}\Omega = (1+(-1)^a)(1+(-1)^b)(1+(-1)^c) \times \frac{((a-1)/2)!((b-1)/2)!((c-1)/2)!}{4((a+b+c+1)/2)!} \tag{A.8}$$

where the surface integral is performed over a unit sphere S^2. This is clearly zero when either a, b or c is odd. This further implies that when we have full sky information available then all the multipole parameters can be determined independently. But in reality, we always have a masked sky. In that case, the parameter extraction will depend upon where the series truncates. Thus in principle infinite number of parameters would be needed. But as we have seen that beyond quadrupole the power is small hence we truncated our series at $\ell = 2$. We have also checked the effect of parameter extraction and ℓ value at which the series is terminated. These results are shown for monopole in Table 3.

A.3 Error estimation

In order to estimate the errors in the extracted parameters, we perform simulations using the following algorithm, summarized in Fig. 5.

1. The monopole, dipole and quadrupole components from the data map are extracted using Eq. (A.3). These multipoles are then used to prepare a full sky map $\mathbb{F}$ at `NSIDE` 64. Note that $\mathbb{F}$ is an exact map featuring the input multipoles.
2. To account for shot-noise in each pixel, we call Poisson distribution with mean $N_{\rm p}$, where $N_{\rm p}$ is the value in pixel 'p' in map $\mathbb{F}$. Next, to include partial-to-full-sky construction uncertainty, we apply the survey mask and extract multipoles again using Eq. (A.3).
3. The previous step is repeated 10,000 times which gives a distribution for various extracted multipoles. The distribution, which is found to be Gaussian, is shown in Fig. 4. From this distribution, we can calculate relevant quantities of interest – mean μ and error σ.

References

1. C.A.P. Bengaly, R. Maartens, M.G. Santos, JCAP **1804**(04), 031 (2018). https://doi.org/10.1088/1475-7516/2018/04/031
2. T. Nadolny, R. Durrer, M. Kunz, H. Padmanabhan, JCAP **11**, 009 (2021). https://doi.org/10.1088/1475-7516/2021/11/009
3. Y. Kim, C.G. Park, H. Noh, J. Hwang, Astron. Astrophys. **660**, A139 (2022). https://doi.org/10.1051/0004-6361/202141909
4. C. Bengaly, Phys. Dark Univ. **35**, 100966 (2022). https://doi.org/10.1016/j.dark.2022.100966
5. O. Lahav, NATO Sci. Ser. C **565**, 131 (2001). https://doi.org/10.1007/978-94-010-0540-1_7

6. P.K. Aluri et al., (2022)
7. S. Ghosh, P. Jain, G. Kashyap, R. Kothari, S. Nadkarni-Ghosh, P. Tiwari, J. Astrophys. Astron. **37**(4), 1 (2016). https://doi.org/10.1007/s12036-016-9395-8
8. C.A.P. Bengaly, R. Maartens, N. Randriamiarinarivo, A. Baloyi, JCAP **09**, 025 (2019). https://doi.org/10.1088/1475-7516/2019/09/025
9. S. Weinberg, *Cosmology* (Oxford University Press, Oxford, 2008)
10. N. Horstmann, Y. Pietschke, D.J. Schwarz, (2021)
11. A. Kogut, C. Lineweaver, G.F. Smoot, C.L. Bennett, A. Banday et al., ApJ **419**, 1 (1993). https://doi.org/10.1086/173453
12. G. Hinshaw, J.L. Weiland, R.S. Hill, N. Odegard, C. Larson et al., ApJS **180**, 225 (2009). https://doi.org/10.1088/0067-0049/180/2/225
13. N.J. Secrest, S. von Hausegger, M. Rameez, R. Mohayaee, S. Sarkar, Astrophys. J. Lett. **937**(2), L31 (2022). https://doi.org/10.3847/2041-8213/ac88c0
14. A.K. Singal, ApJL **742**, L23 (2011). https://doi.org/10.1088/2041-8205/742/2/L23
15. C. Gibelyou, D. Huterer, MNRAS **427**, 1994 (2012). https://doi.org/10.1111/j.1365-2966.2012.22032.x
16. M. Rubart, D.J. Schwarz, A&A **555**(A117) (2013). https://doi.org/10.1051/0004-6361/201321215
17. P. Tiwari, R. Kothari, A. Naskar, S. Nadkarni-Ghosh, P. Jain, Astropart. Phys. **61**, 1 (2015). https://doi.org/10.1016/j.astropartphys.2014.06.004
18. N.J. Secrest, S. von Hausegger, M. Rameez, R. Mohayaee, S. Sarkar, J. Colin, Astrophys. J. Lett. **908**(2), L51 (2021). https://doi.org/10.3847/2041-8213/abdd40
19. F. Marocco, P.R.M. Eisenhardt, J.W. Fowler, J.D. Kirkpatrick, A.M. Meisner, E.F. Schlafly, S.A. Stanford, N. Garcia, D. Caselden, M.C. Cushing, R.M. Cutri, J.K. Faherty, C.R. Gelino, A.H. Gonzalez, T.H. Jarrett, R. Koontz, A. Mainzer, E.J. Marchese, B. Mobasher, D.J. Schlegel, D. Stern, H.I. Teplitz, E.L. Wright, Astrophys. J. Suppl. Ser. **253**(1), 8 (2021). https://doi.org/10.3847/1538-4365/abd805
20. C. Blake, J. Wall, Nature **416**, 150 (2002)
21. F. Crawford, ApJ **692**, 887 (2009). https://doi.org/10.1088/0004-637X/692/1/887
22. P. Tiwari, A. Nusser, J. Cosmol. Astropart. Phys. **2016**(03), 062 (2016). https://doi.org/10.1088/1475-7516/2016/03/062. http://stacks.iop.org/1475-7516/2016/i=03/a=062
23. J. Colin, R. Mohayaee, M. Rameez, S. Sarkar, Mon. Not. R. Astron. Soc. **471**, 1045 (2017). https://doi.org/10.1093/mnras/stx1631
24. N. Aghanim et al., Astron. Astrophys. **641**, A1 (2020). https://doi.org/10.1051/0004-6361/201833880
25. P. Tiwari, P. Jain, Mon. Not. R. Astron. Soc. **447**, 2658 (2015). https://doi.org/10.1093/mnras/stu2535
26. J.J. Condon, W.D. Cotton, E.W. Greisen, Q.F. Yin, R.A. Perley, G.B. Taylor, J.J. Broderick, AJ **115**(5), 1693 (1998). https://doi.org/10.1086/300337. http://stacks.iop.org/1538-3881/115/i=5/a=1693
27. J. Darling, Astrophys. J. Lett. **931**(2), L14 (2022). https://doi.org/10.3847/2041-8213/ac6f08
28. M. Lacy et al., Publ. Astron. Soc. Pac. **132**(1009), 035001 (2020). https://doi.org/10.1088/1538-3873/ab63eb
29. D. McConnell et al., Publ. Astron. Soc. Austral. **37**, e048 (2020). https://doi.org/10.1017/pasa.2020.41
30. A. Nusser, P. Tiwari, ApJ **812**(1), 85 (2015). https://doi.org/10.1088/0004-637X/812/1/85
31. P. Tiwari, G.B. Zhao, A. Nusser, ApJ **943**(2), 116 (2023). https://doi.org/10.3847/1538-4357/acacf8
32. C.G. Park, H. Hyun, H. Noh, J. Hwang, Mon. Not. R. Astron. Soc. **469**(2), 1924 (2017). https://doi.org/10.1093/mnras/stx988
33. H. Eriksen, F. Hansen, A. Banday, K. Górski, P. Lilje, ApJ **605**, 14 (2004). https://doi.org/10.1086/382267
34. H.K. Eriksen, A.J. Banday, K.M. Górski, F.K. Hansen, P.B. Lilje, ApJL **660**, L81 (2007). https://doi.org/10.1086/518091
35. Planck Collaboration, Y. Akrami, M. Ashdown, J. Aumont, C. Baccigalupi, M. Ballardini, A.J. Banday, R.B. Barreiro, N. Bartolo, S. Basak, K. Benabed, M. Bersanelli, P. Bielewicz, J.J. Bock, J.R. Bond, J. Borrill, F.R. Bouchet, F. Boulanger, M. Bucher, C. Burigana, R.C. Butler, E. Calabrese, J.-F. Cardoso, B. Casaponsa, H.C. Chiang, L.P.L. Colombo, C. Combet, D. Contreras, B.P. Crill, P. de Bernardis, G. de Zotti, J. Delabrouille, J.-M. Delouis, E. Di Valentino, J.M. Diego, O. Doré, M. Douspis, A. Ducout, X. Dupac, G. Efstathiou, F. Elsner, T.A. Enßlin, H.K. Eriksen, Y. Fantaye, R. Fernandez-Cobos, F. Finelli, M. Frailis, A.A. Fraisse, E. Franceschi, A. Frolov, S. Galeotta, S. Galli, K. Ganga, R.T. Génova-Santos, M. Gerbino, T. Ghosh, J. González-Nuevo, K.M. Górski, A. Gruppuso, J.E. Gudmundsson, J. Hamann, W. Handley, F.K. Hansen, D. Herranz, E. Hivon, Z. Huang, A.H. Jaffe, W.C. Jones, E. Keihänen, R. Keskitalo, K. Kiiveri, J. Kim, N. Krachmalnicoff, M. Kunz, H. Kurki-Suonio, G. Lagache, J.-M. Lamarre, A. Lasenby, M. Lattanzi, C.R. Lawrence, M. Le Jeune, F. Levrier, M. Liguori, P.B. Lilje, V. Lindholm, M. López-Caniego, Y.-Z. Ma, J.F. Macías-Pérez, G. Maggio, D. Maino, N. Mandolesi, A. Mangilli, A. Marcos-Caballero, M. Maris, P.G. Martin, E. Martínez-González, S. Matarrese, N. Mauri, J.D. McEwen, P.R. Meinhold, A. Mennella, M. Migliaccio, M.-A. Miville-Deschênes, D. Molinari, A. Moneti, L. Montier, G. Morgante, A. Moss, P. Natoli, L. Pagano, D. Paoletti, B. Partridge, F. Perrotta, V. Pettorino, F. Piacentini, G. Polenta, J.-L. Puget, J.P. Rachen, M. Reinecke, M. Remazeilles, A. Renzi, G. Rocha, C. Rosset, G. Roudier, J.A. Rubiño-Martín, B. Ruiz-Granados, L. Salvati, M. Savelainen, D. Scott, E.P.S. Shellard, C. Sirignano, R. Sunyaev, A.-S. Suur-Uski, J.A. Tauber, D. Tavagnacco, M. Tenti, L. Toffolatti, M. Tomasi, T. Trombetti, L. Valenziano, J. Valiviita, B. Van Tent, P. Vielva, F. Villa, N. Vittorio, B.D. Wandelt, I.K. Wehus, A. Zacchei, J.P. Zibin, A. Zonca, A&A **641**, A7 (2020). https://doi.org/10.1051/0004-6361/201935201
36. Planck Collaboration, P.A.R. Ade, N. Aghanim, Y. Akrami, P.K. Aluri, M. Arnaud, M. Ashdown, J. Aumont, C. Baccigalupi, A.J. Banday, et al., A&A **594**, A16 (2016). https://doi.org/10.1051/0004-6361/201526681
37. Planck Collaboration, P.A.R. Ade, N. Aghanim, C. Armitage-Caplan, M. Arnaud, M. Ashdown, F. Atrio-Barandela, J. Aumont, C. Baccigalupi, A.J. Banday, et al., A&A **571**, A23 (2014). https://doi.org/10.1051/0004-6361/201321534
38. J. Hoftuft, H.K. Eriksen, A.J. Banday, K.M. Gorski, F.K. Hansen, P.B. Lilje, Astrophys. J. **699**, 985 (2009). https://doi.org/10.1088/0004-637X/699/2/985
39. J.P. Ralston, P. Jain, IJMPD **13**, 1857 (2004). https://doi.org/10.1142/S0218271804005948
40. P. Jain, J.P. Ralston, MPLA **14**, 417 (1999). https://doi.org/10.1142/S0217732399000481
41. A. de Oliveira-Costa, M. Tegmark, M. Zaldarriaga, A. Hamilton, Phys. Rev. D. **69**(6), 063516 (2004). https://doi.org/10.1103/PhysRevD.69.063516
42. D.J. Schwarz, G.D. Starkman, D. Huterer, C.J. Copi, PhRvL **93**, 221301 (2004). https://doi.org/10.1103/PhysRevLett.93.221301
43. D. Hutsemékers, A&A **332**, 410 (1998)
44. P. Jain, G. Narain, S. Sarala, MNRAS **347**(2), 394 (2004). https://doi.org/10.1111/j.1365-2966.2004.07169.x
45. P. Jain, S. Panda, S. Sarala, PhRvD **66**, 085007 (2002). https://doi.org/10.1103/PhysRevD.66.085007
46. J.A. Morales, D. Saez, Phys. Rev. D **75**, 043011 (2007). https://doi.org/10.1103/PhysRevD.75.043011
47. F.R. Urban, A.R. Zhitnitsky, Phys. Rev. D **82**, 043524 (2010). https://doi.org/10.1103/PhysRevD.82.043524
48. MYu. Piotrovich, Yu.N. Gnedin, T.M. Natsvlishvili, Astrophysics **52**, 451 (2009). https://doi.org/10.1007/s10511-009-9081-5 [Astrofiz.52,451(2009)]

49. N. Agarwal, A. Kamal, P. Jain, Phys. Rev. D **83**, 065014 (2011). https://doi.org/10.1103/PhysRevD.83.065014
50. R. Poltis, D. Stojkovic, Phys. Rev. Lett. **105**, 161301 (2010). https://doi.org/10.1103/PhysRevLett.105.161301
51. E. Hackmann, B. Hartmann, C. Lammerzahl, P. Sirimachan, Phys. Rev. D **82**, 044024 (2010). https://doi.org/10.1103/PhysRevD.82.044024
52. N. Agarwal, P.K. Aluri, P. Jain, U. Khanna, P. Tiwari, EPJC **72**(3), 15 (2012). arXiv:1108.3400
53. P. Tiwari, P. Jain, Mon. Not. R. Astron. Soc. **460**, 2698 (2016). https://doi.org/10.1093/mnras/stw1108
54. P. Tiwari, P. Jain, Mon. Not. R. Astron. Soc. **513**(1), 604 (2022). https://doi.org/10.1093/mnras/stac887
55. C. Gordon, W. Hu, D. Huterer, T. Crawford, Phys. Rev. D. **72**(10), 103002 (2005). https://doi.org/10.1103/PhysRevD.72.103002
56. A.L. Erickcek, S.M. Carroll, M. Kamionkowski, Phys. Rev. D. **78**(8), 083012 (2008). https://doi.org/10.1103/PhysRevD.78.083012
57. L.P. Grishchuk, I.B. Zeldovich, AZh **55**, 209 (1978). [Sov. Astron. **22**, 125 (1978)]
58. L.P. Grishchuk, I.B. Zeldovich, Sov. Ast. **22**, 125 (1978)
59. S. Ghosh, Phys. Rev. D. **89**, 063518 (2014). https://doi.org/10.1103/PhysRevD.89.063518
60. K.K. Das, K. Sankharva, P. Jain, JCAP **2021**(7), 035 (2021). https://doi.org/10.1088/1475-7516/2021/07/035
61. G. Domènech, R. Mohayaee, S.P. Patil, S. Sarkar, JCAP **10**, 019 (2022). https://doi.org/10.1088/1475-7516/2022/10/019
62. P. Tiwari, R. Kothari, P. Jain, Astrophys. J. Lett. **924**(2), L36 (2022). https://doi.org/10.3847/2041-8213/ac447a
63. P.K. Aluri, P. Jain, Mod. Phys. Lett. A **27**, 1250014 (2012). https://doi.org/10.1142/S0217732312500149
64. P. Rath, T. Mudholkar, P. Jain, P. Aluri, S. Panda, J. Cosmol. Astropart. Phys. **4**, 007 (2013). https://doi.org/10.1088/1475-7516/2013/04/007
65. C.B. Collins, S.W. Hawking, Astrophys. J. **180**, 317 (1973). https://doi.org/10.1086/151965
66. R.M. Wald, PhRvD **28**, 2118R (1983)
67. C.B. Collins, J. Math. Phys. **18**, 2116 (1977). https://doi.org/10.1063/1.523191
68. M.S. Turner, L.M. Widrow, Phys. Rev. Lett. **57**, 2237 (1986). https://doi.org/10.1103/PhysRevLett.57.2237
69. G. Leon, E.N. Saridakis, Class. Quantum Gravity **28**, 065008 (2011). https://doi.org/10.1088/0264-9381/28/6/065008
70. C.R. Fadragas, G. Leon, E.N. Saridakis, Class. Quantum Gravity **31**, 075018 (2014). https://doi.org/10.1088/0264-9381/31/7/075018
71. J.A. Stein-Schabes, Phys. Rev. D **35**, 2345 (1987). https://doi.org/10.1103/PhysRevD.35.2345
72. L.G. Jensen, J.A. Stein-Schabes, in *International School of Particle Astrophysics: Gauge Theory and the Early Universe* (1986), pp. 343–352. https://doi.org/10.2172/5716501
73. G.F.R. Ellis, J.E. Baldwin, MNRAS **206**, 377 (1984)
74. P. Tiwari, S. Ghosh, P. Jain, Astrophys. J. **887**, 175 (2019). https://doi.org/10.3847/1538-4357/ab54c8
75. E.L. Wright, P.R.M. Eisenhardt, A.K. Mainzer, M.E. Ressler, R.M. Cutri, T. Jarrett, J.D. Kirkpatrick, D. Padgett, R.S. McMillan, M. Skrutskie, S.A. Stanford, M. Cohen, R.G. Walker, J.C. Mather, D. Leisawitz, I. Gautier, Thomas N., I. McLean, D. Benford, C.J. Lonsdale, A. Blain, B. Mendez, W.R. Irace, V. Duval, F. Liu, D. Royer, I. Heinrichsen, J. Howard, M. Shannon, M. Kendall, A.L. Walsh, M. Larsen, J.G. Cardon, S. Schick, M. Schwalm, M. Abid, B. Fabinsky, L. Naes, C.W. Tsai, AJ **140**(6), 1868 (2010). https://doi.org/10.1088/0004-6256/140/6/1868
76. A. Mainzer, J. Bauer, T. Grav, J. Masiero, R.M. Cutri, J. Dailey, P. Eisenhardt, R.S. McMillan, E. Wright, R. Walker, R. Jedicke, T. Spahr, D. Tholen, R. Alles, R. Beck, H. Brandenburg, T. Conrow, T. Evans, J. Fowler, T. Jarrett, K. Marsh, F. Masci, H. McCallon, S. Wheelock, M. Wittman, P. Wyatt, E. DeBaun, G. Elliott, D. Elsbury, T. Gautier, S. Gomillion, D. Leisawitz, C. Maleszewski, M. Micheli, A. Wilkins, Astrophys. J. **731**(1), 53 (2011). https://doi.org/10.1088/0004-637x/731/1/53
77. A. Mainzer, J. Bauer, R.M. Cutri, T. Grav, J. Masiero, R. Beck, P. Clarkson, T. Conrow, J. Dailey, P. Eisenhardt, B. Fabinsky, S. Fajardo-Acosta, J. Fowler, C. Gelino, C. Grillmair, I. Heinrichsen, M. Kendall, J.D. Kirkpatrick, F. Liu, F. Masci, H. McCallon, C.R. Nugent, M. Papin, E. Rice, D. Royer, T. Ryan, P. Sevilla, S. Sonnett, R. Stevenson, D.B. Thompson, S. Wheelock, D. Wiemer, M. Wittman, E. Wright, L. Yan, Astrophys. J. **792**(1), 30 (2014). https://doi.org/10.1088/0004-637x/792/1/30
78. D. Stern, R.J. Assef, D.J. Benford, A. Blain, R. Cutri, A. Dey, P. Eisenhardt, R.L. Griffith, T.H. Jarrett, S. Lake, F. Masci, S. Petty, S.A. Stanford, C.W. Tsai, E.L. Wright, L. Yan, F. Harrison, K. Madsen, ApJ **753**(1), 30 (2012). https://doi.org/10.1088/0004-637X/753/1/30
79. N.J. Secrest, R.P. Dudik, B.N. Dorland, N. Zacharias, V. Makarov, A. Fey, J. Frouard, C. Finch, Astrophys. J. Suppl. Ser. **221**(1), 12 (2015). https://doi.org/10.1088/0067-0049/221/1/12
80. K.M. Górski, E. Hivon, A.J. Banday, B.D. Wandelt, F.K. Hansen, M. Reinecke, M. Bartelmann, ApJ **622**, 759 (2005). https://doi.org/10.1086/427976
81. A. Zonca, L. Singer, D. Lenz, M. Reinecke, C. Rosset, E. Hivon, K. Gorski, J. Open Source Softw. **4**(35), 1298 (2019). https://doi.org/10.21105/joss.01298
82. B. Carroll, D. Ostlie, *An Introduction to Modern Astrophysics* (Cambridge University Press, 2017). https://books.google.co.in/books?id=PY0wDwAAQBAJ
83. P. Virtanen, R. Gommers, T.E. Oliphant, M. Haberland, T. Reddy, D. Cournapeau, E. Burovski, P. Peterson, W. Weckesser, J. Bright, S.J. van der Walt, M. Brett, J. Wilson, K.J. Millman, N. Mayorov, A.R.J. Nelson, E. Jones, R. Kern, E. Larson, C.J. Carey, İ. Polat, Y. Feng, E.W. Moore, J. VanderPlas, D. Laxalde, J. Perktold, R. Cimrman, I. Henriksen, E.A. Quintero, C.R. Harris, A.M. Archibald, A.H. Ribeiro, F. Pedregosa, P. van Mulbregt, SciPy 1.0 Contributors, Nature Methods **17**, 261 (2020). https://doi.org/10.1038/s41592-019-0686-2
84. J.D. Hunter, Comput. Sci. Eng. **9**(3), 90 (2007). https://doi.org/10.1109/MCSE.2007.55
85. C.R. Harris, K.J. Millman, S.J. van der Walt, R. Gommers, P. Virtanen, D. Cournapeau, E. Wieser, J. Taylor, S. Berg, N.J. Smith, R. Kern, M. Picus, S. Hoyer, M.H. van Kerkwijk, M. Brett, A. Haldane, J.F. del Río, M. Wiebe, P. Peterson, P. Gérard-Marchant, K. Sheppard, T. Reddy, W. Weckesser, H. Abbasi, C. Gohlke, T.E. Oliphant, Nature **585**(7825), 357 (2020). https://doi.org/10.1038/s41586-020-2649-2